Calculation of fine-structure splittings in high-lying ^2F states of rubidium

S. A. Blundell*
Univ. Grenoble Alpes, INAC-SCIB, F-38000 Grenoble, France
and CEA, INAC-SCIB, F-38000 Grenoble, France
(Received 25 August 2014; published 31 October 2014)

We present relativistic many-body calculations of the fine-structure splittings of the $n\,^2F$ Rydberg states of Rb ($n = 4$–16) using both order-by-order relativistic many-body perturbation theory (RMBPT), up to a subset of fourth-order corrections, and relativistic equation-of-motion coupled-cluster methods, including singles, doubles, and an approximate treatment of valence triples. Good overall agreement is found with the measurements of Brandenberger *et al.* [Phys. Rev. A **65**, 042510 (2002); **81**, 032515 (2010)] to better than the 1% level, which is our expected level of theoretical uncertainty due to omitted higher-order correlation effects. It is shown that the RMBPT of the fine-structure splittings is complex and slowly convergent, and that relativistic effects are enhanced compared with the RMBPT of the ionization energy of the ^2F states. We also analyze smaller field-theoretic contributions to the fine-structure splittings from retardation and the radiative self-energy and vacuum polarization, finding them to enter at the 0.1% level.

DOI: 10.1103/PhysRevA.90.042514 PACS number(s): 31.10.+z, 31.15.aj, 31.15.am, 31.15.bw

I. INTRODUCTION

It has long been realized that the fine-structure splitting in heavy alkali-metal atoms, an inherently relativistic effect, can be strongly modified by correlation corrections beyond a mean-field model of the atom such as the Hartree-Fock [1–3] model. A striking example is provided by the measurements of fine-structure splittings in ^2F Rydberg states of rubidium (Rb) by Brandenberger *et al.* [4,5], who used a three-step laser excitation with cycling transitions to achieve a precision of better than 0.1% in the measured splittings of the lower-lying states. The $n\,^2F_{7/2}$ level was found to be lower than the $n\,^2F_{5/2}$ level, the inverse of the fine-structure ordering in hydrogen, and the fine-structure splittings scaled neither as $1/n^3$, as in hydrogen, nor as $1/(n-\delta)^3$, where δ is the quantum defect, as they do to quite good accuracy in the ^2P, ^2D, and ^2F series of lighter alkali metals (see, for example, Ref. [6], and references therein). This is a clear indication that correlation effects play a very important role in the ^2F splittings of Rb.

However, the theory of fine-structure splittings in atoms with more than a few electrons continues to present a challenge for existing methods of atomic theory because of the combination of strong correlation and relativity, and the precise data for the ^2F states of Rb [4,5] mentioned above remain unexplained. In this paper, we apply modern methods of relativistic atomic many-body theory in a detailed study of the ^2F fine-structure splittings of Rb. In lowest order, we assume a relativistic Hartree-Fock (Dirac-Fock) model; then we evaluate higher-order terms in relativistic many-body perturbation theory (MBPT) using relativistic finite basis sets. We consider order-by-order MBPT, as well as relativistic coupled-cluster (CC) methods, which allow for the summation of large subclasses of many-body terms to all orders of perturbation theory. This is shown to lead to an understanding of the observed fine-structure splittings and their trends at a level of 1% (or better). We show that the relativistic MBPT of the splittings is complex and slowly convergent, with high-order CC terms arising from triple excitations, which represent the state-of-the-art in CC methods for medium-to-heavy alkali-metal atoms, entering the fine-structure splittings at the 4% level. Also, relativistic many-body effects are found to be enhanced, including relativistic correlation corrections arising from the Breit interaction (magnetic interactions) among electrons.

The plan of the paper is as follows. In Sec. II A, we give a brief overview of the relativistic MBPT and CC methods used, including a newly developed relativistic equation-of-motion CC method, which is particularly suited to extracting medium-high-lying excited (Rydberg) states. The need to calculate such Rydberg states also places high demands on the quality of the relativistic basis sets employed, and these issues are discussed in Sec. II B. The results along with some discussion are then given in Sec. III A, where we also analyze the phenomenon of the inversion of the splittings, followed by calculations of ionization energies for comparison in Sec. III B. Some smaller effects, such as the isotope shifts and the radiative self-energy and vacuum polarization, are then taken up in Sec. III C and a discussion of various scaling properties of the fine-structure splittings is given in Sec. III D. The conclusions are given in Sec. IV.

II. FORMALISM AND METHODOLOGY

A. Relativistic many-body formalism

The ^2F states of Rb consist of a single valence f electron outside a closed-shell 36-electron Kr-like core. We describe the atom in lowest order by a V^{N-1} (Coulomb) Dirac-Fock (DF) approximation, based on the DF potential for the atomic core. The single-particle states ϕ_i satisfy

$$\left(h_D - \frac{Z(r)}{r} + V_{\rm DF}\right)\phi_i = \varepsilon_i \phi_i, \tag{1}$$

where h_D is the Dirac Hamiltonian, $-Z(r)/r$ is the nuclear Coulomb potential including finite nuclear size, and $V_{\rm DF}$ is the core DF potential

$$\langle i|V_{\rm DF}|j\rangle = \sum_c (g_{icjc} - g_{iccj}). \tag{2}$$

*steven.blundell@cea.fr

The sum in Eq. (2) is over states c in the atomic core (excluding the valence electron) and g_{ijkl} is a Coulomb matrix element,

$$g_{ijkl} = \langle ij|r_{12}^{-1}|kl\rangle. \tag{3}$$

Here and in the following we use atomic units (a.u.), $|e| = m_e = \hbar = 4\pi\epsilon_0 = 1$.

To improve systematically upon this approximation, we use methods of relativistic many-body perturbation theory (RMBPT) [7]. We thus make the "no-virtual-pair" approximation of suppressing the negative-energy states of the Dirac-Fock spectrum with total energy (including rest-mass energy) $\varepsilon_i < -m_e c^2$ and take the electron-electron interaction to be instantaneous. In some parts of the calculation we shall generalize the two-body interaction g_{ijkl} to include also the Breit interaction, which is an instantaneous approximation to transverse-photon exchange [7]. Smaller field-theoretic effects, including retardation (Sec. II A) or the radiative self-energy and vacuum polarization (Sec. III C), will then be added by considering low orders of quantum electrodynamic perturbation theory.

We calculate the the fine-structure splitting $\Delta E(nF)$ as a difference of ionization energies $-E(nF_j)$,

$$\Delta E(nF) = E(nF_{7/2}) - E(nF_{5/2}). \tag{4}$$

This difference is calculated separately at each level of approximation (DF level, second-order RMBPT, etc.) and tested carefully for numerical significance. Below we present formulas for the (negative of the) ionization energy E_v of a general valence state v, where v will be taken to be the $nf_{7/2}$ or $nf_{5/2}$ state required for the difference (4).

In order-by-order MBPT, the lowest-order approximation to the valence ionization energy is the valence eigenvalue of the V^{N-1} DF equations, $E_v^{(0)} = \varepsilon_v$, and the first-order valence ionization energy $E_v^{(1)}$ in this potential vanishes [8]. The leading correlation term is the second-order energy,

$$E_v^{(2)} = \langle v|\Sigma^{(2)}(\varepsilon_v)|v\rangle, \tag{5}$$

where $\Sigma^{(2)}$ is the second-order many-body self-energy operator (to be distinguished from the radiative self-energy discussed in Sec. III C), which is given by [8,9]

$$\langle i|\Sigma^{(2)}(\omega)|j\rangle = \sum_{amr} \frac{g_{rmja}(g_{iarm} - g_{iamr})}{\omega + \varepsilon_a - \varepsilon_r - \varepsilon_m} - \sum_{abm} \frac{g_{imab}(g_{abjm} - g_{abmj})}{\varepsilon_a + \varepsilon_b - \omega - \varepsilon_m}. \tag{6}$$

Here a and b are core states, m and r are excited states above the core (including the valence state v), and i and j are general states. The sum over excited states r and m, which in RMBPT are restricted to the bound and positive-energy continuum branch of the DF spectrum, is performed using a relativistic finite basis set constructed from B splines [10].

The third-order ionization energy $E_v^{(3)}$ is given by a sum of 12 Brueckner-Goldstone diagrams, the evaluation of which is discussed in Refs. [7,11]. However, studies of heavy alkali-metal atoms [11] have shown that, in general, the third-order valence ionization energy $E_v^{(3)}$ does not significantly improve upon the second-order energy $E_v^{(2)}$; to obtain improvement for a neutral atom, it is usually necessary to include subclasses of slowly convergent higher-order terms summed to all orders of perturbation theory. One such subclass consists of chains of second-order self-energy units $\Sigma^{(2)}$, which bring in important terms from fourth-, sixth-, eighth-, ..., order perturbation theory. We define the all-order sum of these diagrams of fourth and higher order to be $E_v^{(4\mathrm{ch})}$, which is calculated as described in Ref. [7].

The chaining of the many-body self-energy is one example of a subset of many-body terms summed to all orders of perturbation theory. To obtain higher accuracy, it is necessary to sum further subclasses of RMBPT terms. The CC approach [12,13] is a formalism for performing such all-order sums in a complete and systematic way. One of the first relativistic implementations of such an all-order method for atoms was given in Refs. [14,15], which used a Fock-space coupled-cluster (FS-CC) scheme [8,16,17] to compute valence ionization energies and other properties of alkali-metal atoms, including single and double excitations of core and valence states to all orders of MBPT. The method of Ref. [15] omitted nonlinear CC terms, but it did include a subset of valence triple excitations (an excitation involving one valence and two core electrons). Later relativistic atomic FS-CC work included the nonlinear CC terms [18–21] and provided more complete (but still partial) treatments of triple excitations [22,23].

In this work we employ an equation-of-motion coupled-cluster (EOM-CC) approach (reviewed in Ref. [13]) in the electron-attachment (EA-EOM-CC) form of Nooijen and Bartlett [24], which is suitable for describing valence ionization energies of one-valence-electron atoms. Our version of EA-EOM-CC is relativistic and adapted to atoms. We include all single and double excitations (with all possible nonlinear CC terms), and a partial treatment of valence triple excitations. A detailed presentation of this recently developed approach will be given elsewhere; here we provide a only brief summary of the main points. Note that a relativistic single-reference EOM-CC method was recently presented [25,26] that is suitable for calculating excited states of closed-shell atoms.

The EOM method was initially developed in nuclear physics by Rowe and co-workers [27], and there were also applications in quantum chemistry during the same period (for example, Ref. [28]). In EOM approaches, one expresses the state of interest as $|\Psi_k\rangle = \Omega_k|\Psi_0\rangle$, in terms of an excitation operator Ω_k acting on a (fully correlated) reference state $|\Psi_0\rangle$. The operator Ω_k satisfies

$$[H,\Omega_k]|\Psi_0\rangle = \omega_k|\Psi_0\rangle, \tag{7}$$

which effectively acts as an eigenvalue equation for Ω_k with eigenvalues $\omega_k = E_k - E_0$, where $H|\Psi_k\rangle = E_k|\Psi_k\rangle$ and $H|\Psi_0\rangle = E_0|\Psi_0\rangle$. In practical schemes, the reference state $|\Psi_0\rangle$ must be approximated and the operator Ω_k truncated. CC methods were incorporated into the EOM approach by using an exponential ansatz for the reference state $|\Psi_0\rangle$ having the general form $|\Psi_0\rangle = \exp(T)|0\rangle$, where $|0\rangle$ is a mean-field state and the operator T is suitably truncated [29,30]. The steps required to extend EOM-CC methodology to the calculation of matrix elements are reviewed in Ref. [13].

Following the EA-EOM-CC approach [24], we take the reference state to be the ground state of the closed-shell

$(N-1)$-electron core (that is, with no valence electron present)

$$|\Psi_0\rangle = e^T|0\rangle, \tag{8}$$

where here $|0\rangle$ is the ground-state V^{N-1} DF determinant of the core, and T is the core CC operator (with no valence electron present)

$$T = \sum_{ma} t_a^m a_m^\dagger a_a + \frac{1}{4}\sum_{mrab} t_{ab}^{mr} a_m^\dagger a_r^\dagger a_b a_a + \cdots, \tag{9}$$

with the excitation amplitudes t_a^m, t_{ab}^{mr}, ..., etc., satisfying the usual single-reference CC equations [8,13]. Here and below, a,b, ..., etc., signify core states, and m, r, ..., etc., excited states (above the core). In this work we truncate T at double excitations (CCSD level).

Following the EA-EOM-CC approach [24], the excitation operator Ω_k is then taken to be

$$\Omega_k = \sum_m \rho^m(k) a_m^\dagger + \frac{1}{2}\sum_m \rho_a^{mr}(k) a_m^\dagger a_r^\dagger a_a + \cdots. \tag{10}$$

The overall effect of Ω_k is to add one electron to the state it acts on, so that $|\Psi_k\rangle$ has N electrons while the core state $|\Psi_0\rangle$ has $(N-1)$. In the first instance we truncate Ω_k at the second term in (10), which corresponds to valence doubles (an excitation of one valence and one core electron) and yields the EA-EOM-CCSD scheme. The excitation amplitudes $\rho^m(k)$, $\rho_a^{mr}(k)$, ..., etc., in Eq. (10) are found by diagonalizing the nonsymmetric matrix [24]

$$\bar{H}_{\alpha\beta} = \langle 0|\hat{\alpha}(\bar{H}\hat{\beta}^\dagger)_C|0\rangle, \tag{11}$$

yielding eigenvalues ω_k and eigenvectors $\rho_\alpha(k)$,

$$\bar{H}_{\alpha\beta}\,\rho_\beta(k) = \omega_k \rho_\alpha(k). \tag{12}$$

In Eqs. (11) and (12), $\bar{H} = e^{-T}He^T$ is the similarity-transformed Hamiltonian, the subscript C indicates connected terms only, and α and β are used to denote generically all possible single, double, ..., etc., excitations in Ω_k, with $\hat{\alpha}^\dagger$ and $\hat{\beta}^\dagger$ the corresponding excitation operators (e.g., $\hat{\beta}^\dagger = a_m^\dagger a_r^\dagger a_a$ for a valence doubles electron-attachment excitation $a \to mr$). The index $k = 0,1,2,\ldots$ is used to label the eigenvalues of $\bar{H}_{\alpha\beta}$. The lowest eigenvalue $k = 0$ corresponds to the ground state of the N-electron atom, and the low-lying excited states ($k = 1,2,\ldots$) correspond to dominant configurations in which the valence electron is singly excited (thus, the $5s$ electron in Rb is excited to the $5p_{1/2}$, $5p_{3/2}$, ..., etc., states). Since E_0 here is the total energy of the $(N-1)$-electron core, $\omega_k = E_k - E_0$ is the valence ionization energy for these low-lying states. Note that the ground-state eigenvalue ω_0 is nonzero and gives the ground-state valence ionization energy.

From the point of view of configuration interaction, the EA-EOM-CCSD scheme includes not only all single and double excitations of the N-electron atom, but also the dominant quadruple excitations, which arise from disconnected products $(1/2)T_2^2$ or $T_2(\Omega_k)_2$ of the two-body parts of T and Ω_k [8,13]. The dominant triple excitations, however, correspond to connected diagrams [8,13], and for the highest accuracy these must be included explicitly in the procedure. Unfortunately, simply adding the next (third) term on the right-hand sides of Eqs. (9) and (10) (which would yield the EA-EOM-CCSDT approach [31]) is computationally too demanding for all but the smallest atoms. In this work, we therefore continue to truncate the core excitations T at double excitations (CCSD level), and construct approximations for the effect of valence triple excitations.

Triple excitations can be regarded as perturbing the singles and doubles amplitudes, giving contributions that we refer to as T_S and T_D, respectively. When these terms are added to the EA-EOM-CCSD equations, one obtains what we shall refer to as the EA-EOM-CCSDT$_{\rm SD}$ approach. A detailed description of this procedure will be given elsewhere. The derivation of expressions for T_S and T_D is analogous to the way the triples perturbation of single excitations was derived in Ref. [15] in the context of FS-CC; the approach also follows the same general lines as the CCSDT-1 approximation in single-reference (closed-shell) CC theory [32]. Methods for constructing triples approximations in EA-EOM-CC theory have also been discussed in Ref. [33]. The many-body content of our partial-triples scheme is close to that of the atomic FS-CC approaches of Refs. [22,23]. Note that we here include only *valence triples* in this way (triple excitations involving the valence electron and two core electrons); examples of MBPT diagrams containing such excitations are given in Fig. 1.

The leading omissions in our EA-EOM-CCSDT$_{\rm SD}$ approach are thus: (i) connected core triple excitations (excitation of three core electrons), and (ii) connected quadruple excitations, of which the dominant terms are expected to be connected valence quadruples (an excitation of the valence electron and three core electrons, described by a connected MBPT diagram). In general, in an alkali-metal atom the effect of valence excitations is expected to dominate that of pure core excitations of the same rank (single, double, etc.), in part because the excitation energy associated with a valence excitation is significantly less than that for excitation from the core (see, for example, Ref. [11]).

As in the RMBPT approach, we make the no-virtual-pair approximation, restricting all states to the positive-energy branch (core and excited) of the DF spectrum as given by a relativistic B-spline finite basis set [10]. The two-body interaction is taken to be pure Coulomb (3). Eigenvalues and eigenvectors are extracted from $\bar{H}_{\alpha\beta}$ by a nonsymmetric

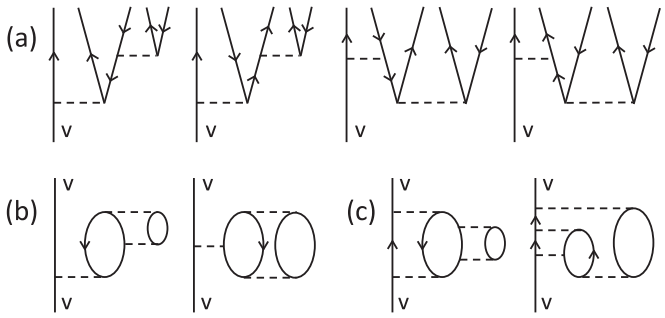

FIG. 1. (a) Connected valence triple excitations for a valence state v in third-order MBPT; (b) and (c) show, respectively, examples of third- and fourth-order valence-ionization-energy diagrams that involve a valence triples excitation. The diagrams in (b) and (c) would be absent in the EA-EOM-CCSD approach, but are picked up in the present approach (together with higher-order diagrams).

subspace-iteration algorithm [34]. For the present work, we require the lowest 13 eigenvalues with $f_{7/2}$ or $f_{5/2}$ valence symmetry ($4\,^2F$ to $16\,^2F$ Rydberg states), which can all be readily converged to ten or more digits of accuracy (for a given basis set). It can be shown that the EA-EOM-CCSD approach should give valence ionization energies in exact agreement with those of the FS-CCSD approach for a single valence electron [(1,0) sector of Fock space], both for the ground state and, in principle, also for the low-lying excited states [24,35]. However, the many-body diagrams for $\bar{H}_{\alpha\beta}$ given by Eq. (11) are organized in a sufficiently different way from those of the FS-CCSD method that numerical agreement between the two methods is not completely trivial. One of the debugging tests we used while developing our EA-EOM-CCSD approach was to compare low-lying valence ionization energies with those given by an older FS-CCSD code, finding better than ten-digit agreement with identical basis sets.

The approximate expressions for valence triples depend on the singles and doubles amplitudes in the operators T and Ω_k (as do the analogous terms in Ref. [15] and the CCSDT-1 single-reference method [32]). Thus, it is possible to evaluate the valence triples perturbatively (noniteratively), by solving the EA-EOM-CCSD equations once and using these amplitudes to evaluate the valence-triples energy contributions. Alternatively, they can be evaluated iteratively, with the triples-perturbed singles and doubles amplitudes being reinserted into the triples terms and the process iterated to self-consistency. As we shall see, in the present application the iteration of triples to self-consistency leads to a significant additional contribution.

So far, relativistic effects have been included by using single-particle states that are solutions of the DF equations (1), but the electron-electron interaction (3) has been taken to be purely Coulombic. Further relativistic effects can be introduced by generalizing the two-body interaction (3) to include the Breit interaction B_{12} [7],

$$g_{ijkl} \to \langle ij|r_{12}^{-1}|kl\rangle + \langle ij|B_{12}|kl\rangle, \tag{13}$$

which describes magnetic electron-electron interactions.

As we will see in Sec. III, in the present application the effect of the Breit interaction is not negligible, but quite small (of order 1.5% of the fine-structure splittings in lowest order). Since as we will see $E_v^{(2)} + E_v^{(3)} + E_v^{(4\mathrm{ch})}$ accounts for 90% or more of Coulomb correlation corrections to fine-structure splittings, we assume here that it is sufficient to evaluate Breit correlation corrections at the same level. The procedure we use to do this is as follows. First, we solve the DF equations (1) with the generalized two-body interaction (13) (the Breit-Coulomb DF equations), yielding modified eigenvalues ε_i and basis states ϕ_i. The lowest-order Breit correction ε_v^B is defined as the shift in the valence eigenvalue,

$$\varepsilon_v \to \varepsilon_v + \varepsilon_v^B, \tag{14}$$

where ε_v on the right-hand side of Eq. (14) is now understood as the purely Coulombic valence DF eigenvalue, and ε_v^B is the modification due to including the Breit interaction (13). Similarly, each higher-order RMBPT term acquires a correction defined by

$$E_v^{(2)} \to E_v^{(2)} + B_v^{(2)}, \tag{15}$$

$$E_v^{(3)} \to E_v^{(3)} + B_v^{(3)}, \tag{16}$$

$$E_v^{(4\mathrm{ch})} \to E_v^{(4\mathrm{ch})} + B_v^{(4\mathrm{ch})}. \tag{17}$$

These corrections arise both from using the generalized two-body interaction (13) in the RMBPT expressions, and at the same time replacing all single-particle states and energies in these expressions by their Breit-Coulomb DF counterparts.

To relax the approximation of instantaneous electron-electron interactions, we calculate the lowest-order retardation correction arising from one-photon exchange between valence and core using the method of Ref. [7]. Higher-order Coulomb corrections to retardation may be included by analyzing retardation corrections to the self-consistent Breit-Coulomb DF equations [36], and we use this approach also. However, the higher-order corrections turn out to be small, and the overall size of retardation is only about 0.1% of the fine-structure splittings (see Sec. III).

B. Numerical procedure and uncertainties

The relativistic B-spline basis set [10] is set up by placing the atom in a cavity, so that the continuum states are discretized. The cavity radius must be sufficiently large so as not to "compress" the highest-lying Rydberg states of interest ($16f_{5/2}$ and $16f_{7/2}$), and in addition the number of basis states N_f included in the f-wave channels ($f_{5/2}$ and $f_{7/2}$) must be sufficiently large that the highest-lying Rydberg state is accurately reproduced. We use a cavity radius of $750a_0$ and $N_f = 90$ for f-wave states, which accurately reproduces DF eigenvalues and fine-structure splittings for all Rydberg states 4–$16f$, the fine-structure splittings being in agreement with the DF values to better than 10^{-11} a.u. For the other (non-f-wave) states, we use a cavity radius in the range 20–$40a_0$ with $N = 20$–60 basis states in each angular-momentum channel ($s_{1/2}$, $p_{1/2}$, $p_{3/2}$, ..., etc.), the precise values depending on the quantity being calculated.

Since we calculate fine-structure splittings by direct subtraction of ionization energies [Eq. (4)], it is important to test the sensitivity of the differences $\Delta X(nF) = X(nF_{7/2}) - X(nF_{5/2})$ to the numerical parameters defining the basis set (and thereby optimize the basis set) for any given quantity X of interest (e.g., $E^{(2)}$, $E^{(3)}$, CC correlation energies, etc.). The relevant parameters include the cavity radius, the number and distribution of B-spline knot points, and the degree k of the B-spline polynomials. In this way, a reasonably reliable estimate of basis-set numerical uncertainty can be made.

An important source of basis-set uncertainty is related to the upper angular-momentum cutoff of states included in the calculation. We proceed by initially truncating the basis at some orbital angular momentum l_0, including all states with $l \leqslant l_0$ in the calculation of any given quantity $Y(l_0)$. The calculation is then repeated for $l_0 = 3,4,\ldots,l_{\max}$, yielding a series of results $Y(3), Y(4), \ldots, Y(l_{\max})$ which is then extrapolated to $l_{\max} \to \infty$ (usually by fitting to polynomials in $1/l_0$). We take $l_{\max} = 11$ (o states) for $E^{(2)}$, $E^{(3)}$, $E^{(4\mathrm{ch})}$, and

the corresponding Breit RMBPT contributions, and $l_{\max} = 7$ (k states) in CC calculations. The lower $l_{\max}$ for CC work was partly a compromise to limit computer time and memory, but interestingly it turns out that the l_0 series is more rapidly convergent for CC fine-structure splittings than for $\Delta E^{(2)}$, $\Delta E^{(3)}$, or $\Delta E^{(4\mathrm{ch})}$. The third-order fine-structure splitting $\Delta E^{(3)}$ has a particularly slow l_0 convergence, which can be traced specifically to the diagram involving two bubbles [11]. The all-order sum of such bubble diagrams included in the CC approach has a significantly improved high-l_0 behavior.

In general, fine-structure splittings place greater demands on the basis set than the individual $n\,^2F_{7/2}$ or $n\,^2F_{5/2}$ ionization energies, requiring higher values of $l_{\max}$ and greater numbers N of basis states in each angular-momentum channel to achieve a given fractional accuracy. We optimized basis-set parameters for fine-structure calculations. The numerical uncertainty is dominated by that arising from the N truncation and the extrapolation to $l_{\max} \to \infty$, the latter typically being slightly smaller than the former for fine-structure splittings (but much smaller for ionization energies). Possible numerical uncertainty arising from the radial grids used to store radial wave functions and from the degree of convergence of iterative processes (e.g., in extracting CC energies or $E^{(4\mathrm{ch})}$) is negligible. The final numerical uncertainties in the CC calculations, quoted in the result tables, are around 0.3% of the fine-structure splittings and 0.01% of the ionization energies.

III. RESULTS AND DISCUSSION

A. Fine-structure splittings

Table I shows RMBPT calculations of the fine-structure splittings. Each column of the table corresponds to the difference of the corresponding quantities for ionization energies, $\Delta X(nF) = X(nF_{7/2}) - X(nF_{5/2})$, and the negative value of the final total signifies that the $n\,^2F_{7/2}$ levels are below the $n\,^2F_{5/2}$, in agreement with the observations for ^2F states in Rb (see Refs. [4,5], and references therein) but inverting the (Dirac) ordering in hydrogen.

This inversion of the fine-structure levels is seen to be present already at DF level, and can be understood in greater detail as follows. The DF potential is the sum of direct and exchange potentials, $V_{\mathrm{DF}} = V_{\mathrm{DF}}^{\mathrm{dir}} + V_{\mathrm{DF}}^{\mathrm{exch}}$, where $V_{\mathrm{DF}}^{\mathrm{dir}}$ is the spherically symmetric classical electrostatic potential due to the DF atomic core, and

$$\langle i|V_{\mathrm{DF}}^{\mathrm{exch}}|k\rangle = -\sum_c g_{icck}. \tag{18}$$

Thus, the valence DF eigenvalue separates into two terms,

$$\begin{aligned} \varepsilon_v &= \varepsilon_v^{\mathrm{dir}} + \varepsilon_v^{\mathrm{exch}}, \\ \varepsilon_v^{\mathrm{dir}} &= \langle v|h_D - Z(r)/r + V_{\mathrm{DF}}^{\mathrm{dir}}|v\rangle, \\ \varepsilon_v^{\mathrm{exch}} &= \langle v|V_{\mathrm{DF}}^{\mathrm{exch}}|v\rangle. \end{aligned} \tag{19}$$

The direct potential $V_{\mathrm{DF}}^{\mathrm{dir}}$ is a scalar with no explicit dependence on total angular momentum j; the direct term above contributes $\varepsilon^{\mathrm{dir}}(4f_{7/2}) - \varepsilon^{\mathrm{dir}}(4f_{5/2}) = +0.049\ \mu$Ha to the $4\,^2F$ fine-structure splitting, which has the same sign and order of magnitude as the Dirac fine-structure splitting of the $4f$ levels in hydrogen, $+0.035\ \mu$Ha. However, the angular-momentum structure of the exchange integrals in $\langle v|V_{\mathrm{DF}}^{\mathrm{exch}}|v\rangle$ [Eq. (18)] yields a strongly j-dependent term. We find an exchange fine-structure splitting $\varepsilon^{\mathrm{exch}}(4f_{7/2}) - \varepsilon^{\mathrm{exch}}(4f_{5/2}) = -0.191\ \mu$Ha, which thus inverts the fine-structure levels and gives the final DF value of $0.049 - 0.191 = -0.142\ \mu$Ha. The exchange interaction of the valence f states is greatest with the $4p_{1/2}$ and $4p_{3/2}$ core states, which together contribute 98.5% of the total exchange fine-structure splitting (see also the discussion of fine-structure inversion in Refs. [1–3,37].)

Although the ordering of the $n\,^2F_{7/2}$ and $n\,^2F_{5/2}$ levels is correct at DF level, the DF fine-structure values are still about 25% discrepant with experiment (for all principal quantum numbers $n = 4$–16), which must be accounted for by higher-order correlation effects. The majority of the correlation effect is picked up by the second-order RMBPT term $\Delta E^{(2)}$ in Table I, which reduces the fractional discrepancy Δ with experiment to about 7%, as shown in Fig. 2. Here and later we define $\Delta = (E_{\mathrm{theory}} - E_{\mathrm{expt.}})/E_{\mathrm{expt.}}$. A further improvement to a discrepancy of about 2.5% is then found at the correlation level $\Delta E^{(2)} + \Delta E^{(3)} + \Delta E^{(4\mathrm{ch})}$. Note, however, the slow and irregular convergence of order-by-order RMBPT seen in

TABLE I. RMBPT calculations of the fine-structure splittings of the $n\,^2F$ states. Notation: DF, Dirac-Fock value; $\Delta E^{(m)}$, contribution of mth-order RMBPT with Coulomb interaction (see text); Transverse, sum of Breit contributions and retardation (from Table II); Total (4ch), sum of all previous contributions. Estimated numerical uncertainties are given in parentheses. Units: 10^{-6} a.u. (μHa).

n	DF	$\Delta E^{(2)}$	$\Delta E^{(3)}$	$\Delta E^{(4\mathrm{ch})}$	Transverse	Total (4ch)
4	−0.142 44	0.021 87(9)	−0.003 70(13)	0.010 33(4)	0.000 50(2)	−0.113 45(16)
5	−0.127 39	0.017 81(7)	−0.003 34(12)	0.008 64(3)	0.000 54(2)	−0.103 73(14)
6	−0.092 56	0.012 66(5)	−0.002 49(9)	0.006 20(2)	0.000 42(1)	−0.075 78(10)
7	−0.065 80	0.008 96(4)	−0.001 81(6)	0.004 39(2)	0.000 30(1)	−0.053 96(8)
8	−0.047 43	0.006 46(3)	−0.001 33(5)	0.003 16(1)	0.000 22(1)	−0.038 92(5)
9	−0.034 96	0.004 77(2)	−0.000 99(3)	0.002 32(1)	0.000 16	−0.028 69(4)
10	−0.026 35	0.003 60(1)	−0.000 75(3)	0.001 75(1)	0.000 12	−0.021 63(3)
11	−0.020 28	0.002 78(1)	−0.000 58(2)	0.001 34(1)	0.000 10	−0.016 65(2)
12	−0.015 91	0.002 19(1)	−0.000 46(2)	0.001 05	0.000 07	−0.013 06(2)
13	−0.012 69	0.001 75(1)	−0.000 37(1)	0.000 84	0.000 06	−0.010 41(2)
14	−0.010 27	0.001 42(1)	−0.000 30(1)	0.000 68	0.000 05	−0.008 43(1)
15	−0.008 42	0.001 16	−0.000 25(1)	0.000 56	0.000 04	−0.006 91(1)
16	−0.006 99	0.000 97	−0.000 21(1)	0.000 46	0.000 03	−0.005 74(1)

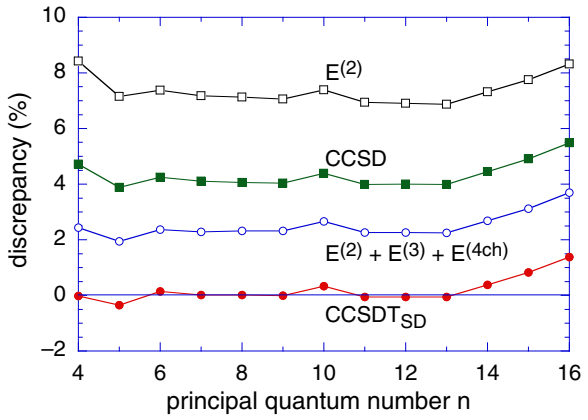

FIG. 2. (Color online) Fractional discrepancy with experiment of theoretical $n\,^2F$ fine-structure splittings calculated at various levels: second-order RMBPT (empty squares), second-order plus third-order plus chained fourth-order RMBPT (empty circles), CCSD (full squares), and $\mathrm{CCSDT_{SD}}$ (full circles).

Table I: $\Delta E^{(4\mathrm{ch})}$ is about 50% of $\Delta E^{(2)}$ and about three times larger than $\Delta E^{(3)}$. In view of this, the 2.5% level of discrepancy found is perhaps slightly fortuitous.

The RMBPT contributions discussed so far assume a pure Coulomb interaction (3) among electrons. Since the fine-structure splitting is an inherently relativistic effect, it might be expected that transverse-photon exchange (magnetic interactions) among the atomic electrons should play a relatively important role in correlation effects. The transverse-photon term included in Table I is broken down into individual contributions in Table II. The lowest-order Breit fine-structure contribution, derived from the Breit-Coulomb DF eigenvalue modifications ε_v^B (14), is about -1.5% of the fine-structure splittings. Higher-order Breit correlation effects are also important, the Breit correlation terms $\Delta B^{(2)} + \Delta B^{(3)} + \Delta B^{(4\mathrm{ch})}$ (15)–(17) contributing about $+1\%$ of the fine-structure splittings, and partially compensating the lowest-order effect, so that overall the Breit contribution is about -0.5% of the fine-structure splitting. We also include in Table II the contribution of retardation at DF level (see Sec. II A), which is a small effect of order -0.1% of the fine-structure splittings.

The slow and irregular convergence of RMBPT noted above motivates use of the more complete all-order treatment of correlation effects provided by CC methods. The results of our CC calculations are summarized in Tables III and IV and in Fig. 2. The relativistic EA-EOM-CCSD approach, which sums single and double excitations to all orders, is seen to give a discrepancy with experiment of about 4%. Adding valence triples, which is the most computationally demanding step in this work and leads to the most complete approach considered, the EA-EOM-$\mathrm{CCSDT_{SD}}$ approach, then improves the discrepancy with experiment to better than 0.5% in most cases (see Fig. 3).

In the EA-EOM-$\mathrm{CCSDT_{SD}}$ approach just discussed, we iterate the valence triples to self-consistency, but a less computationally demanding approach is to evaluate them perturbatively (or noniteratively), as discussed in Sec. II A. If we evaluate perturbatively just the expensive T_D term (giving the effect of triple excitations on double excitations) and continue to include T_S iteratively, we find a final discrepancy with experiment of about 1.7%. Thus, the iteration to convergence of the T_D term is significant, giving a contribution of about -1.5% of the fine-structure splittings. In fact, the term T_D alone is quite large, about -10% of fine-structure splittings (T_D tends to cancel partially with T_S so that valence triples overall are about a -4% effect). Thus, it is not really surprising that iterations of T_D produce shifts in the results at the 1% level.

B. Ionization energies

While the experiments of Brandenberger *et al.* [4,5] are primarily concerned with fine-structure splittings, it is also possible to infer the ionization energies of the $n\,^2F$ states from their data, for comparison with our theoretical predictions. Ionization energies turn out to be a much less sensitive test of correlation and relativistic effects than fine-structure splittings.

The experiment [4,5] involves a three-step excitation: (i) from the upper ground-state hyperfine level to a $5P_{3/2}$ hyperfine level with a laser of wavelength $\lambda_1^{\mathrm{air}} = 780.03$ nm

TABLE II. Contributions to fine-structure splittings of the $n\,^2F$ states from transverse-photon exchange. Notation: BC-DF, value at Breit-Coulomb DF level, from ε_v^B in Eq. (14); $\Delta B^{(m)}$, contributions from mth-order RMBPT, Eqs. (15)–(17); Retardation, total retardation contribution; Total, sum of all previous terms. Estimated numerical uncertainties are given in parentheses. Units: 10^{-6} a.u. (μHa).

n	BC-DF	$\Delta B^{(2)}$	$\Delta B^{(3)}$	$\Delta B^{(4\mathrm{ch})}$	Retardation	Total
4	0.001 87	−0.001 21(2)	−0.000 09(1)	−0.000 23	0.000 15	0.000 50(2)
5	0.001 52	−0.000 89(2)	−0.000 04	−0.000 18	0.000 12	0.000 54(2)
6	0.001 08	−0.000 60(1)	−0.000 02	−0.000 13	0.000 09	0.000 42(1)
7	0.000 76	−0.000 42(1)	−0.000 01	−0.000 09	0.000 06	0.000 30(1)
8	0.000 54	−0.000 29(1)	−0.000 01	−0.000 06	0.000 04	0.000 22(1)
9	0.000 40	−0.000 21	0.000 00	−0.000 05	0.000 03	0.000 16
10	0.000 30	−0.000 16	0.000 00	−0.000 04	0.000 02	0.000 12
11	0.000 23	−0.000 12	0.000 00	−0.000 03	0.000 02	0.000 10
12	0.000 18	−0.000 10	0.000 00	−0.000 02	0.000 01	0.000 07
13	0.000 14	−0.000 08	0.000 00	−0.000 02	0.000 01	0.000 06
14	0.000 12	−0.000 06	0.000 00	−0.000 01	0.000 01	0.000 05
15	0.000 09	−0.000 05	0.000 00	−0.000 01	0.000 01	0.000 04
16	0.000 08	−0.000 04	0.000 00	−0.000 01	0.000 01	0.000 03

TABLE III. Coupled-cluster calculations of the fine-structure splittings of the $n\,^2F$ states. Notation: DF, Dirac-Fock value; CCSD, correlation energy at singles and doubles level; $\mathrm{CCSDT_{SD}}$, correlation energy including also valence triples; Transverse, sum of Breit contributions and retardation (from Table II); Total CCSD or $\mathrm{CCSDT_{SD}}$, sum of DF value, Transverse, and corresponding CC correlation energy. Estimated numerical uncertainties are given in parentheses. Units: 10^{-6} a.u. (μHa).

n	DF	CCSD	$\mathrm{CCSDT_{SD}}$	Transverse	Total CCSD	Total $\mathrm{CCSDT_{SD}}$
4	−0.142 44	0.025 97(21)	0.031 21(34)	0.000 50(2)	−0.115 97(21)	−0.110 73(34)
5	−0.127 39	0.021 14(17)	0.025 45(28)	0.000 54(2)	−0.105 70(17)	−0.101 39(28)
6	−0.092 56	0.015 01(12)	0.018 06(20)	0.000 42(1)	−0.077 14(12)	−0.074 09(20)
7	−0.065 80	0.010 58(8)	0.012 73(14)	0.000 30(1)	−0.054 92(8)	−0.052 76(14)
8	−0.047 43	0.007 62(6)	0.009 16(10)	0.000 22(1)	−0.039 59(6)	−0.038 05(10)
9	−0.034 96	0.005 62(4)	0.006 75(7)	0.000 16	−0.029 17(5)	−0.028 04(7)
10	−0.026 35	0.004 24(3)	0.005 09(6)	0.000 12	−0.021 99(3)	−0.021 13(6)
11	−0.020 28	0.003 26(3)	0.003 92(4)	0.000 10	−0.016 93(3)	−0.016 27(4)
12	−0.015 91	0.002 56(2)	0.003 07(3)	0.000 07	−0.013 28(2)	−0.012 76(3)
13	−0.012 69	0.002 04(2)	0.002 45(3)	0.000 06	−0.010 59(2)	−0.010 18(3)
14	−0.010 27	0.001 65(1)	0.001 98(2)	0.000 05	−0.008 57(1)	−0.008 24(2)
15	−0.008 42	0.001 35(1)	0.001 63(2)	0.000 04	−0.007 03(1)	−0.006 76(2)
16	−0.006 99	0.001 12(1)	0.001 35(1)	0.000 03	−0.005 84(1)	−0.005 61(1)

(in air); (ii) then to a $4D_{5/2}$ hyperfine level with a wavelength $\lambda_2^{\mathrm{air}} = 1528.99$ nm; and (iii) finally to the $n\,^2F_{7/2}$ or $n\,^2F_{5/2}$ levels with a wavelength λ_3^{air} depending on principal quantum number n. The ionization energy $-E(nF)$ of the final $n\,^2F$ state of ^{87}Rb can then be inferred as

$$-E(nF) = E_0(5S) - \Delta E_{\mathrm{hfs}}(5S) - hc\left(\frac{1}{\lambda_1} + \frac{1}{\lambda_2} + \frac{1}{\lambda_3}\right), \qquad (20)$$

where $E_0(5S) = 4.177\,127\,06(10)$ eV is the ionization energy of the ground $5S$ state (lower hyperfine level), $\Delta E_{\mathrm{hfs}}(5S) = 6834.68$ MHz is the ground-state hyperfine splitting (data from Ref. [38]), and λ_1, λ_2, and λ_3 are the above wavelengths in vacuum. We convert the air wavelengths to vacuum using the tabulation of Ref. [39], finding $\lambda_1 = 780.237$ nm and $\lambda_2 = 1529.404$ nm. The final values of $E(nF)$ obtained for each n are summarized in Table V. Nominal experimental uncertainties are assigned to each ionization energy by assuming an uncertainty of 0.01 nm (1 in the last quoted digit) in each of λ_1^{air}, λ_2^{air}, and λ_3^{air}; these nominal uncertainties are around 2 μHa, which is 20–400 times larger than the fine-structure splittings, so for the purpose of this section there is no distinction between the $n\,^2F_{7/2}$ and $n\,^2F_{5/2}$ levels.

Table VI summarizes the RMBPT calculations of the ionization energies, and Table VII the CC calculations (see also Ref. [21] for $n \leqslant 10$). Unlike the case with fine-structure splittings, relativistic contributions to ionization energies in neutral Rb are small. The lowest-order Breit contribution (at Breit-Coulomb DF level) is about 100–1000 times smaller than the nominal experimental errors (depending on n), so we omit transverse-photon contributions throughout. Moreover, we see from Table VII that the ionization energy in lowest

TABLE IV. Comparison of theoretical fine-structure splittings of $n\,^2F$ states with experiment. Notation: DF, Dirac-Fock value; Total (2), second-order RMBPT (sum of DF, $\Delta E^{(2)}$, and Transverse in Table I); Total (4ch), RMBPT up to chained fourth-order terms (final column in Table I); Total CCSD or $\mathrm{CCSDT_{SD}}$, coupled-cluster values from Table III; Expt., experimental fine-structure splittings from Refs. [4] and [5]. Estimated numerical uncertainties (in theoretical values) are given in parentheses. Units: 10^{-6} a.u. (μHa).

n	DF	Total (2)	Total (4ch)	Total CCSD	Total $\mathrm{CCSDT_{SD}}$	Expt.
4	−0.142 44	−0.120 07(9)	−0.113 45(16)	−0.115 97(21)	−0.110 73(34)	−0.110 75(8)
5	−0.127 39	−0.109 03(7)	−0.103 73(14)	−0.105 70(17)	−0.101 39(28)	−0.101 75(6)
6	−0.092 56	−0.079 49(5)	−0.075 78(10)	−0.077 14(12)	−0.074 09(20)	−0.074 03(3)
7	−0.065 80	−0.056 54(4)	−0.053 96(8)	−0.054 92(8)	−0.052 76(14)	−0.052 75(3)
8	−0.047 43	−0.040 75(3)	−0.038 92(5)	−0.039 59(6)	−0.038 05(10)	−0.038 04(3)
9	−0.034 96	−0.030 02(2)	−0.028 69(4)	−0.029 17(5)	−0.028 04(7)	−0.028 04(5)
10	−0.026 35	−0.022 62(1)	−0.021 63(3)	−0.021 99(3)	−0.021 13(6)	−0.021 06(3)
11	−0.020 28	−0.017 41(1)	−0.016 65(2)	−0.016 93(3)	−0.016 27(4)	−0.016 28(3)
12	−0.015 91	−0.013 65(1)	−0.013 06(2)	−0.013 28(2)	−0.012 76(3)	−0.012 77(5)
13	−0.012 69	−0.010 88(1)	−0.010 41(2)	−0.010 59(2)	−0.010 18(3)	−0.010 18(3)
14	−0.010 27	−0.008 81(1)	−0.008 43(1)	−0.008 57(1)	−0.008 24(2)	−0.008 21(5)
15	−0.008 42	−0.007 22	−0.006 91(1)	−0.007 03(1)	−0.006 76(2)	−0.006 70(3)
16	−0.006 99	−0.005 99	−0.005 74(1)	−0.005 84(1)	−0.005 61(1)	−0.005 53(3)

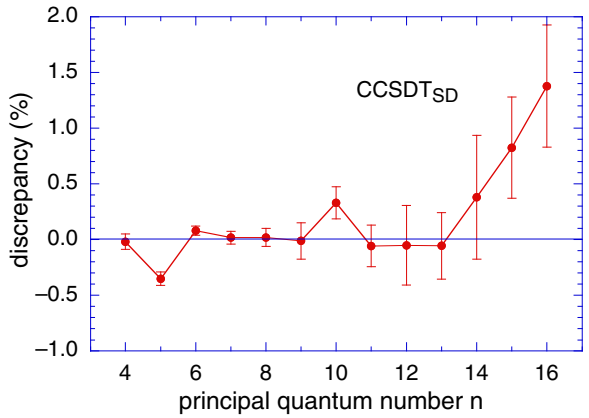

FIG. 3. (Color online) Fractional discrepancy with experiment of theoretical $n\,^2F$ fine-structure splittings calculated at CCSDT$_{SD}$ level. Error bars indicate the experimental uncertainty. Note that the calculation is also subject to theoretical uncertainty (not shown), including numerical basis-set truncation uncertainties of order 0.3% (see text).

order, DF level, is already quite accurate, ranging from about 0.6% discrepant with experiment for $n = 4$ to about 1–2 experimental standard deviations discrepant for $n = 15$ and 16. Accordingly, the lower n levels provide the most stringent test of the many-body theory.

From Table VI we see that the $E^{(2)}$ correlation level agrees quite well with experiment, although this is largely fortuitous, as shown by the fact that at the $E^{(2)} + E^{(3)} + E^{(4ch)}$ correlation level there is a small systematic discrepancy with experiment (for the lower n values). This discrepancy is removed at CCSD and CCSDT$_{SD}$ level, where good agreement is found with experiment for all $n = 4$–16 at the level of experimental and numerical uncertainty. Note that the valence triples contribution, given by the difference of the CCSDT$_{SD}$ and CCSD columns in Table VII, is barely significant for any n at the level of these uncertainties.

TABLE V. Experimental ionization energies $-E(nF)$ of the $n\,^2F$ states of ^{87}Rb. Wavelengths λ_3 (see text) in air are taken from Refs. [4] and [5] and converted to vacuum using the tabulation in Ref. [39]. Nominal experimental uncertainties (see text) are included in parentheses in the last column.

n	λ_3 (air) (nm)	λ_3 (vac) (nm)	$E(nF)$ (a.u.)
4	1344.28	1344.65	−0.031 432(2)
5	1007.53	1007.81	−0.020 107(2)
6	886.85	887.09	−0.013 955(2)
7	827.14	827.37	−0.010 247(2)
8	792.53	792.75	−0.007 842(2)
9	770.44	770.65	−0.006 194(2)
10	755.38	755.59	−0.005 015(2)
11	744.62	744.83	−0.004 144(2)
12	736.64	736.84	−0.003 481(2)
13	730.54	730.74	−0.002 965(2)
14	725.78	725.98	−0.002 556(2)
15	721.99	722.19	−0.002 226(2)
16	718.90	719.10	−0.001 955(2)

C. Smaller effects

We consider in this section several smaller effects that are small or negligible, and have been omitted from the main tabulations in the previous sections. First, the finite nuclear mass (nuclear recoil) leads to corrections E_{mass} to ionization energies E of order $E_{mass} \approx -(m_e/M_{nuc})E \approx -6 \times 10^{-6} E$. Calculations at DF level confirm that nuclear recoil modifies the fine-structure splittings at a similar fractional level, and is thus completely negligible at the level of experimental uncertainty.

A small field-theoretic term, retardation, was included in Table II and found to enter at about −0.1% of the fine-structure splittings. This suggests that it would be interesting to check the order of magnitude of the radiative self-energy (SE) and vacuum polarization (VP) contributions, which are other field-theoretic effects. We estimated these effects using the method of Ref. [40]. Since f electrons have a very small probability density at small r (in the region of order one Compton wavelength around the nucleus that is important for the SE and VP), the lowest-order valence SE and VP turn out to be negligible. However, the dominant contribution to SE and VP is instead found to arise from the core-relaxation term, a many-body term giving the change in the (much larger) core SE and VP as the valence electron changes during a transition, here $nf_{5/2}$ to $nf_{7/2}$. As was discussed in Sec. III A in connection with the inversion of the fine-structure splittings, the dominant j-dependent core-valence interaction is the exchange interaction (18), the contribution of the $4p$ core states being the largest. Similarly, we find that the dominant SE and VP contribution to the fine-structure splittings is the exchange-interaction core-relaxation term [40] arising from the $4p$ core electrons (mostly $4p_{1/2}$). Unfortunately, the method of Ref. [40] was adapted to highly charged ions, not neutral atoms, and the values obtained here are rather sensitive to the choice of core potential and other parameters. Nevertheless, the results suggest that the total SE and VP contribution could be of the same order of magnitude, or slightly smaller, than retardation, entering at the level of $\lesssim$0.1% of the fine-structure splittings. In general, more research is required on methods of calculating these radiative corrections in neutral atoms with more than a few electrons.

In the first experimental paper [4], some measurements of fine-structure splittings were made in ^{85}Rb as well as ^{87}Rb, but the differences found (the isotope effect) were not statistically significant at the level of experimental uncertainty. As we have seen above, the mass isotope effect (change in nuclear-recoil contribution) is negligible. Calculations at DF level show that the field isotope effect (due to the change in nuclear mean-square charge radius) enters at the level of 10^{-6} of the fine-structure splittings, and is therefore also negligible. A third possible source of isotope effect is the hyperfine interaction. The three-step laser excitation procedure selects a subset of possible hyperfine transitions [4,5], and if the final line profile is slightly asymmetric, the line "center" could implicitly contain a first-order hyperfine contribution. However, we find (at CCSD level) that the hyperfine constants

TABLE VI. RMBPT calculations of the ionization energies of the $n\,^2F$ states. Notation: DF, Dirac-Fock value ε_v; $E^{(m)}$, contribution of mth-order RMBPT with Coulomb interaction (see text); Total (2), second-order RMBPT (sum of DF and $E^{(2)}$); Total (4ch), RMBPT up to chained fourth-order terms (sum of DF, $E^{(2)}$, $E^{(3)}$, and $E^{(4ch)}$). The values given correspond to the negative of the ionization energy. Estimated numerical uncertainties are given in parentheses. Units: a.u. (Ha).

n	ε_v (DF)	$E^{(2)}$	$E^{(3)}$	$E^{(4ch)}$	Total (2)	Total (4ch)
4	−0.031 257	−0.000 173(1)	0.000 017(1)	−0.000 006	−0.031 431(1)	−0.031 420(1)
5	−0.020 006	−0.000 098	0.000 011(1)	−0.000 004	−0.020 104(1)	−0.020 097(1)
6	−0.013 893	−0.000 061	0.000 007	−0.000 003	−0.013 954	−0.013 950
7	−0.010 207	−0.000 040	0.000 005	−0.000 002	−0.010 247	−0.010 244
8	−0.007 815	−0.000 027	0.000 003	−0.000 001	−0.007 842	−0.007 840
9	−0.006 174	−0.000 019	0.000 002	−0.000 001	−0.006 194	−0.006 193
10	−0.005 001	−0.000 014	0.000 002	−0.000 001	−0.005 016	−0.005 015
11	−0.004 133	−0.000 011	0.000 001	−0.000 001	−0.004 144	−0.004 143
12	−0.003 473	−0.000 008	0.000 001	0.000 000	−0.003 481	−0.003 481
13	−0.002 959	−0.000 007	0.000 001	0.000 000	−0.002 966	−0.002 965
14	−0.002 551	−0.000 005	0.000 001	0.000 000	−0.002 557	−0.002 556
15	−0.002 223	−0.000 004	0.000 001	0.000 000	−0.002 227	−0.002 227
16	−0.001 953	−0.000 004	0.000 000	0.000 000	−0.001 957	−0.001 957

of the $4F$ and $5F$ levels (where this effect would be most significant) are of order 0.1 MHz or smaller (see also Ref. [21]), and the hyperfine splittings in these levels are thus comparable to or smaller than the experimental uncertainty in the position of the line center (∼0.4 MHz). These results are consistent with the experimental observation of no significant isotope effect, as well as with the highly symmetric observed line shape and the failure to observe hyperfine splittings.

D. Scaling properties of fine-structure splittings

A striking property of the fine-structure results in Figs. 2 and 3 is that the fractional discrepancy with experiment at any given correlation level (DF, $E^{(2)}$, etc.) is largely independent of principal quantum number n. Closer inspection of Tables I–III reveals that, for each correlation term ΔX (such as $\Delta E^{(2)}$, $\Delta E^{(3)}$, etc.), the ratio $\Delta X/\Delta\varepsilon_{\rm DF}$ is nearly independent of n, where $\Delta\varepsilon_{\rm DF}$ is the DF-level result. For example, one finds that for all $n = 6$–16,

$$-0.1383 \leqslant \Delta E^{(2)}/\Delta\varepsilon_{\rm DF} \leqslant -0.1361, \qquad (21)$$

with $\Delta E^{(2)}/\Delta\varepsilon_{\rm DF} = -0.1535$ (for $n = 4$) and -0.1398 (for $n = 5$) deviating slightly from the pattern. Since $\Delta\varepsilon_{\rm DF}$ itself differs from experiment $\Delta E_{\rm expt.}$ by a nearly constant fraction, one finds also that $\Delta E^{(2)}/\Delta E_{\rm expt.}$ is nearly independent of n.

These scaling properties can be understood by observing that at short range (of the order of the atomic core radius, or slightly larger), the radial wave functions of the valence f states have nearly the same shape (independent of n) and differ to a good approximation only by a normalization factor. To see this, we show large (upper Dirac component) radial wave functions for $nf_{5/2}$ DF valence states in Fig. 4. One sees that the main peak in the wave function moves outward as expected as n increases (the radius of a Bohr orbit is

TABLE VII. Coupled-cluster calculations of the ionization energies of the $n\,^2F$ states. Notation: DF, Dirac-Fock value ε_v; CCSD, correlation energy with singles and doubles; $\rm CCSDT_{SD}$, correlation energy including also valence triples; Total CCSD or $\rm CCSDT_{SD}$, sum of DF value and corresponding CC correlation energy; Expt., experimental ionization energies from Table V. The values given correspond to the negative of the ionization energy. Estimated numerical uncertainties (in theoretical values) are given in parentheses. Units: a.u. (Ha).

n	ε_v (DF)	CCSD	$\rm CCSDT_{SD}$	Total CCSD	Total $\rm CCSDT_{SD}$	Expt.
4	−0.031 257	−0.000 173(2)	−0.000 172(2)	−0.031 431(2)	−0.031 429(2)	−0.031 432(2)
5	−0.020 006	−0.000 098(1)	−0.000 101(1)	−0.020 104(1)	−0.020 107(1)	−0.020 107(2)
6	−0.013 893	−0.000 060(1)	−0.000 064(1)	−0.013 954(1)	−0.013 957(1)	−0.013 955(2)
7	−0.010 207	−0.000 039	−0.000 042	−0.010 246	−0.010 249	−0.010 247(2)
8	−0.007 815	−0.000 027	−0.000 029	−0.007 841	−0.007 843	−0.007 842(2)
9	−0.006 174	−0.000 019	−0.000 021	−0.006 194	−0.006 195	−0.006 194(2)
10	−0.005 001	−0.000 014	−0.000 015	−0.005 015	−0.005 016	−0.005 015(2)
11	−0.004 133	−0.000 011	−0.000 012	−0.004 144	−0.004 145	−0.004 144(2)
12	−0.003 473	−0.000 008	−0.000 009	−0.003 481	−0.003 482	−0.003 481(2)
13	−0.002 959	−0.000 007	−0.000 007	−0.002 966	−0.002 966	−0.002 965(2)
14	−0.002 551	−0.000 005	−0.000 006	−0.002 557	−0.002 557	−0.002 556(2)
15	−0.002 223	−0.000 004	−0.000 005	−0.002 227	−0.002 227	−0.002 226(2)
16	−0.001 953	−0.000 004	−0.000 004	−0.001 957	−0.001 957	−0.001 955(2)

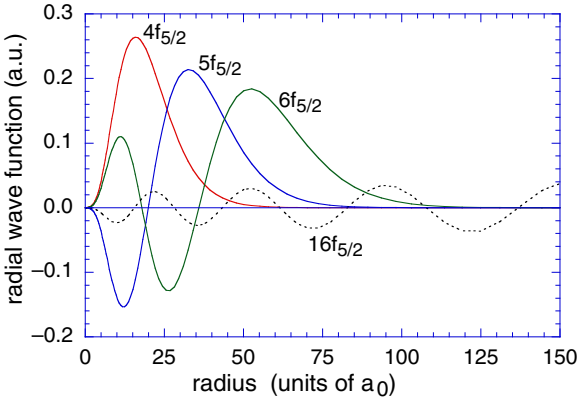

FIG. 4. (Color online) Large radial functions (upper Dirac component) of the $4f_{5/2}$, $5f_{5/2}$, $6f_{5/2}$, and $16f_{5/2}$ valence states. The radius of the atomic core is about $3.5a_0$.

proportional to n^2). But the first peak (maximum or minimum) at small r, which occurs at $r_{\rm peak} \approx 16a_0$ for $n = 4$, moves inward slightly as n increases, reaching an asymptotic value as $n \to \infty$ of $r_{\rm peak} \approx 10a_0$. This asymptotic peak position is that for the state at the ionization threshold with energy zero, and is reached already for $n \gtrsim 6$. For $r \lesssim 10a_0$ we can thus write

$$g_{nf}(r) \approx A_{nf}\, g_{\infty f}(r), \tag{22}$$

where $g_{nf}(r)$ is the radial wave function and A_{nf} is a normalization factor. The radial charge density of the atomic core drops to zero for $r \gtrsim 3.5a_0$, so Eq. (22) is valid inside the atomic core and somewhat beyond.

Now, in general, terms in MBPT for the valence ionization energy (and other atomic properties) can be represented as DF valence expectation values of effective operators [8]. If such an effective operator $\hat{X}$ is of predominantly short range, concentrated inside the atomic core or just outside, from Eq. (22) we would have

$$\langle nf|\hat{X}|nf\rangle \approx A_{nf}^2 \langle \infty f|\hat{X}|\infty f\rangle. \tag{23}$$

We illustrate this property for the second-order ionization energy $E^{(2)}$, the dominant contribution to correlation, which is given by the valence expectation value of the second-order many-body self-energy operator $\Sigma^{(2)}$ (6). In Fig. 5(a) we show plots of the large radial components of the states $|\phi_n\rangle = \Sigma^{(2)}|nf_{5/2}\rangle$ for various n. The states $|\phi_n\rangle$ are peaked at $r \approx 3.2a_0$, close to the edge of the atomic core, implying that $\Sigma^{(2)}$ has a predominantly short range (the long-range part of $\Sigma^{(2)}$, giving polarization or dispersion interactions, here plays a reduced role). If we now scale the states $|\phi_n\rangle$ so that the main peak value is unity, as in Fig. 5(b), we confirm that the shape of the radial functions of $|\phi_n\rangle$ is nearly independent of n, which together with Eq. (22) then implies Eq. (23) for $\hat{X} = \Sigma^{(2)}$. Some deviation in $|\phi_n\rangle$ occurs for $n = 4$ and $n = 5$ in the region $r \gtrsim 10a_0$, where the $4f$ and $5f$ radial wave functions differ somewhat from the asymptotic form (see Fig. 4).

Now, the fine-structure splitting at DF level is calculated as a difference of DF eigenvalues, $\Delta\varepsilon_{\rm DF} = \varepsilon_{7/2} - \varepsilon_{5/2}$. But this difference can, in principle, also be written as a valence expectation value of an effective operator corresponding to

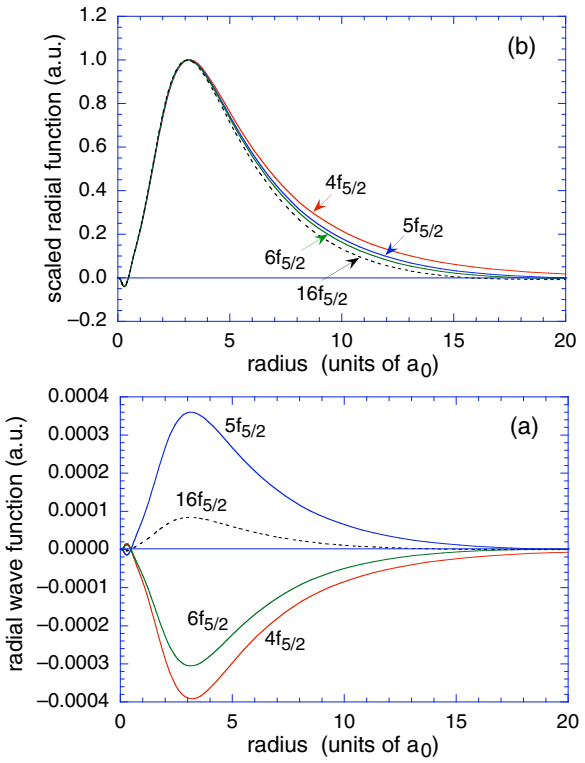

FIG. 5. (Color online) (a) Large Dirac radial function of the states $|\phi_n\rangle$ formed when the second-order many-body self-energy operator $\Sigma^{(2)}$ acts on the $4f_{5/2}$, $5f_{5/2}$, $6f_{5/2}$, and $16f_{5/2}$ valence states. (b) The same states as in (a), but rescaled so that the value at the peak is unity. The radius of the atomic core is about $3.5a_0$.

terms in a nonrelativistic reduction of the DF equations. To the extent that this effective operator also has predominantly short range, as is to be expected, the normalization factor A_{nf}^2 will cancel when one takes the ratio $\Delta E^{(2)}/\Delta\varepsilon_{\rm DF}$, thus explaining why these ratios are observed to be nearly independent of n (at least for $n \geqslant 6$) as in Eq. (21).

It was pointed out by Brandenberger *et al.* [4,5] that their measured fine-structure splittings did not scale with n either as $1/n^3$, the Dirac hydrogenic scaling, or as $1/(n-\delta)^3$, where δ is the quantum defect (and that, in any case, the ordering of the $n\,^2F_{7/2}$ and $n\,^2F_{5/2}$ levels was inverted relative to hydrogen). As we have seen, the main reason for the inversion can be traced to the core-valence exchange interaction, which changes both the sign and the order of magnitude of the lowest-order fine-structure splitting, and further corrections of order 25% then arise from higher-order correlation. After including all these effects in our calculations, we recover the n dependence observed experimentally to high precision.

IV. CONCLUSIONS

We have presented relativistic many-body calculations of the fine-structure splittings of the ^2F Rydberg states of Rb at various correlation levels. The most complete treatment considered was CCSDT$_{\rm SD}$, which includes singles, doubles, and valence triples to all orders in a coupled-cluster framework. From the point of view of configuration interaction, this

approach also includes the dominant quadruple excitations, which arise from *disconnected* products of double excitations. While it is possible to make a reasonably reliable estimate of purely numerical uncertainty (which we found to be about 0.3% of the fine-structure splittings), it is much harder to estimate the uncertainty arising from omitted higher-order correlation effects, here the core triple excitations (excitation of three electrons from the core) and *connected* quadruple excitations. Unfortunately, there are no rigorous bounds on omitted terms in this sort of calculation.

Starting from a Dirac-Fock calculation, which gave discrepancies of about 25% with experiment for the fine-structure splittings, we found that singles and doubles (CCSD) gave about a −20% correlation effect, and valence triples ($\mathrm{CCSDT_{SD}}$) a further −4% correlation effect (see Fig. 2). Based on the apparent degree of convergence in these results, it is not unreasonable to suppose that connected quadruples could enter at the 1% level. Also, the effect of core excitations is generally suppressed in alkali-metal atoms (see, for example, Ref. [11]), so one would expect core triples to be suppressed relative to valence triples, possibly also to the 1% level. Since our final $\mathrm{CCSDT_{SD}}$ fine-structure splittings agree with experiment for the most part to better than 0.5% (see Fig. 3), the overall level of agreement between theory and experiment therefore seems perfectly satisfactory. (It is possible that the level of agreement found for $\mathrm{CCSDT_{SD}}$ is in fact partly fortuitous, in the sense that omitted correlation effects are slightly larger but tend to cancel.) The largest discrepancies at $\mathrm{CCSDT_{SD}}$ level are for the highest $n = 15$ and 16 Rydberg states measured, which are 1%–1.5% discrepant with experiment, but this is only 2–2.5 experimental standard deviations in those measurements.

The *trend* of the discrepancies as a function of n may be significant. We note that the small deviations of the points for the $n = 5$, 10, 14, 15, and 16 Rydberg states observed at $\mathrm{CCSDT_{SD}}$ level in Fig. 3 are also seen to occur in a similar pattern at other correlation levels $E^{(2)}$, $E^{(2)} + E^{(3)} + E^{(4\mathrm{ch})}$, and CCSD in Fig. 2. But, once again, the discrepancies are small compared to possible theoretical uncertainty from omitted correlation effects, so this is not clear.

Our calculations show that the fine-structure splittings are very sensitive to correlation effects: triple excitations with CC methods, which is currently the state of the art, enter at the 4% level. By comparison, triples enter at the 0.02% level in the ^2F-state ionization energies, which have a much more rapidly convergent MBPT. Relativistic many-body effects also are enhanced: the Breit interaction enters at the 0.5%–1.0% level in fine-structure splittings, but only at the level of one part in 10^6 in the ionization energies. Field-theoretic effects such as retardation and the radiative self-energy and vacuum polarization are also enhanced, and are expected to enter the fine-structure splittings at the 0.1% level, which is comparable to the experimental uncertainty at small n (e.g., 0.07% experimental uncertainty for $n = 4$). Unfortunately, in order to isolate these field-theoretic terms in the calculation, it would first be necessary to improve the treatment of correlation effects to a level significantly better than the 1% level currently achieved with $\mathrm{CCSDT_{SD}}$, for example, by including valence quadruples and core triples in some approximation. It is clear that the ^2F-state fine-structure splittings, even in a neutral medium-Z element such as Rb, provide a stringent test of present-day methods in relativistic atomic many-body theory.

ACKNOWLEDGMENTS

We gratefully acknowledge John R. Brandenberger for discusssions regarding the experiment and Dale L. Skran for his special encouragement of this work.

[1] E. Luc-Koenig, Phys. Rev. A **13**, 2114 (1976).
[2] T. Lee, J. E. Rodgers, T. P. Das, and R. M. Sternheimer, Phys. Rev. A **14**, 51 (1976).
[3] N. C. Pyper and P. Marketos, J. Phys. B: At., Mol. Opt. Phys. **14**, 4469 (1981).
[4] J. R. Brandenberger, C. A. Regal, R. O. Jung, and M. C. Yakes, Phys. Rev. A **65**, 042510 (2002).
[5] J. R. Brandenberger and G. S. Malyshev, Phys. Rev. A **81**, 032515 (2010).
[6] J. Farley and R. Gupta, Phys. Rev. A **15**, 1952 (1977).
[7] W. R. Johnson, S. A. Blundell, and J. Sapirstein, Phys. Rev. A **37**, 2764 (1988).
[8] I. Lindgren and J. Morrison, *Atomic Many-Body Theory* (Springer, Berlin, 1986).
[9] S. A. Blundell, D. S. Guo, W. R. Johnson, and J. Sapirstein, At. Data Nucl. Data Tables **37**, 103 (1987).
[10] W. R. Johnson, S. A. Blundell, and J. Sapirstein, Phys. Rev. A **37**, 307 (1988).
[11] S. A. Blundell, W. R. Johnson, and J. Sapirstein, Phys. Rev. A **38**, 4961 (1988).
[12] F. Coester and H. Kümmel, Nucl. Phys. **17**, 477 (1960).
[13] R. J. Bartlett and M. Musiał, Rev. Mod. Phys. **79**, 291 (2007).
[14] S. A. Blundell, W. R. Johnson, Z. W. Liu, and J. Sapirstein, Phys. Rev. A **40**, 2233 (1989).
[15] S. A. Blundell, W. R. Johnson, and J. Sapirstein, Phys. Rev. A **43**, 3407 (1991).
[16] I. Lindgren, Int. J. Quantum Chem. (Suppl.) **12**, 33 (1978).
[17] M. A. Haque and D. Mukherjee, J. Chem. Phys. **80**, 5058 (1984).
[18] E. Ilyabaev and U. Kaldor, Phys. Rev. A **47**, 137 (1993).
[19] R. K. Chaudhuri, P. K. Panda, B. P. Das, U. S. Mahapatra, and D. Mukherjee, Phys. Rev. A **60**, 246 (1999).
[20] R. Pal, M. S. Safronova, W. R. Johnson, A. Derevianko, and S. G. Porsev, Phys. Rev. A **75**, 042515 (2007).
[21] M. S. Safronova and U. I. Safronova, Phys. Rev. A **83**, 052508 (2011).
[22] A. Derevianko, S. G. Porsev, and K. Beloy, Phys. Rev. A **78**, 010503 (2008).
[23] A. Borschevsky, T. Zelovich, E. Eliav, and U. Kaldor, Chem. Phys. **395**, 104 (2012).
[24] M. Nooijen and R. J. Bartlett, J. Chem. Phys. **102**, 3629 (1995).
[25] H. Pathak, B. K. Sahoo, B. P. Das, N. Vaval, and S. Pal, Phys. Rev. A **89**, 042510 (2014).
[26] D. K. Nandy, Y. Singh, and B. K. Sahoo, Phys. Rev. A **89**, 062509 (2014).

[27] D. J. Rowe, Rev. Mod. Phys. **40**, 153 (1968).
[28] T. H. Dunning and V. McKoy, J. Chem. Phys. **47**, 1735 (1967).
[29] K. Emrich, Nucl. Phys. A **351**, 379 (1981).
[30] H. Sekino and R. J. Bartlett, Int. J. Quantum Chem. **18**, 255 (1984).
[31] M. Musiał and R. J. Bartlett, J. Chem. Phys. **119**, 1901 (2003).
[32] Y. S. Lee, S. A. Kucharski, and R. J. Bartlett, J. Chem. Phys. **81**, 5906 (1984).
[33] J. D. Watts and R. J. Bartlett, Chem. Phys. Lett. **258**, 581 (1996).
[34] K. Hirao and H. Nakatsuji, J. Comput. Phys. **45**, 246 (1982).
[35] D. Sinha, S. K. Mukhopadhyay, R. Chaudhuri, and D. Mukherjee, Chem. Phys. Lett. **154**, 544 (1989).
[36] J. D. Gillaspy, D. Osin, Y. Ralchenko, J. Reader, and S. A. Blundell, Phys. Rev. A **87**, 062503 (2013).
[37] I. Lindgren and A.-M. Mårtensson, Phys. Rev. A **26**, 3249 (1982).
[38] D. A. Steck, Rubidium 87 D line data, 2008, http://steck.us/alkalidata/.
[39] B. Edlén, Metrologia **2**, 71 (1966).
[40] S. A. Blundell, Phys. Rev. A **47**, 1790 (1993); Phys. Scr. **T46**, 144 (1993).